Interpretation of Molecular Intracule and Extracule Density Distributions in Terms of Valence Bond Structures: Two-Electron Systems and Processes

Xavier Fradera and Miquel Duran*,†

Institute of Computational Chemistry, University of Girona, 17071 Girona, Catalonia, Spain

Jordi Mestres*,‡

Department of Molecular Design and Informatics, N.V. Organon, 5340 BH Oss, The Netherlands

Received: May 11, 2000

The topological features of molecular intracule and extracule densities and their Laplacian distributions computed at the HF and CISD levels of theory are interpreted in terms of valence bond (VB) structures. By mapping each VB structure of a system onto its intracule and extracule density distributions, the values of the intracule and extracule densities can be associated with the contribution of each VB structure or group of structures to the total wave function. Difference maps between the Laplacian of intracule and extracule densities calculated at the HF and CISD levels are used to identify which VB structures are given more or less weight upon inclusion of electron correlation. As application examples, the topological features of the intracule and extracule density distributions for the H_2 and linear H_3^+ two-electron systems are rationalized in terms of the contributions of different VB structures. Moreover, their respective dissociation reactions, $H_2 \rightarrow H^\bullet + H^\bullet$ and $H_3^+ \rightarrow H_2 + H^+$, have been studied using the same interpretative analysis. The evolution of the values of the intracule and extracule densities, in those points associated with VB structures, is found to be in qualitative agreement with the change of the weight of each VB structure to the total wave function along the reaction coordinate.

Introduction

The topological analysis of one-electron densities is a widely established methodology for analyzing the information contained in the electronic wave functions of molecular systems.[1] In principle, this analysis could be also performed on electron-pair densities. However, molecular electron-pair densities are computationally expensive and the analysis of their topology is complex because they are functions of six variables and, thus, difficult to visualize and analyze in detail.[2]

The intracule, $I(\mathbf{r})$, and extracule, $E(\mathbf{R})$, densities have been proposed as a means for reducing the dimensionality of the electron-pair density, $\Gamma(\mathbf{r}_1,\mathbf{r}_2)$, while still keeping some of the original two-electron character.[3−10] For a pair of electrons, the definition of an intracule coordinate, $\mathbf{r} = \mathbf{r}_1 - \mathbf{r}_2$, and an extracule coordinate, $\mathbf{R} = (\mathbf{r}_1 + \mathbf{r}_2)/2$, leads to the expression of the intracule and extracule densities as

$$I(\mathbf{r}) = \int \Gamma(\mathbf{r}_1,\mathbf{r}_2)\delta((\mathbf{r}_1 - \mathbf{r}_2) - \mathbf{r})\, d\mathbf{r}_1\, d\mathbf{r}_2 \qquad (1)$$

$$E(\mathbf{R}) = \int \Gamma(\mathbf{r}_1,\mathbf{r}_2)\delta\left(\frac{\mathbf{r}_1 + \mathbf{r}_2}{2} - \mathbf{R}\right) d\mathbf{r}_1\, d\mathbf{r}_2 \qquad (2)$$

$I(\mathbf{r})$ and $E(\mathbf{R})$ are the probability density functions for the interparticle distance and for the center of mass of the electron pair, respectively. Some important properties of $I(\mathbf{r})$ are that it is invariant upon translation of the molecule and that it has a center of inversion at the origin. On the other hand, $E(\mathbf{R})$ reflects the spatial arrangement of the nuclear framework and its origin depends on the positioning of the molecule.

Recently, the availability of efficient algorithms for the calculation of $I(\mathbf{r})$ and $E(\mathbf{R})$ in large grids of points[11] has led to the study of the topologies of molecular $I(\mathbf{r})$ and $E(\mathbf{R})$ distributions at the HF level for relatively large systems ($C_3H_3^+$, $C_4H_4^{2+}$, $C_5H_5^-$, and C_6H_6).[12] Using the same methodology, maps of the Laplacian of $I(\mathbf{r})$, $\nabla^2 I(\mathbf{r})$, and the Laplacian of $E(\mathbf{R})$, $\nabla^2 E(\mathbf{R})$, at the HF level have been reported for a series of molecules (C_2H_2, C_2H_4, and C_2H_6).[13] Recently, intracule and extracule density and Laplacian maps have been also presented for the intermediate structures corresponding to the hydride, hydrogen, and proton transfer reactions between two CH_3 groups at a constrained C−C distance,[14] and the electron-pair density redistributions taking place in the H_2/H^+, $H_2/H^\bullet$, and H_2/H^- transfer processes have been also investigated by means of intracule and extracule densities.[15] These studies revealed that the topologies of molecular $I(\mathbf{r})$ and $E(\mathbf{R})$, and specially those of $\nabla^2 I(\mathbf{r})$ and $\nabla^2 E(\mathbf{R})$, are considerably more complex than the topologies of one-electron density and Laplacian distributions, even for small molecules. This is due in part to the fact that, in contrast with one-electron distributions, the topology of electron-pair distributions cannot be directly associated with the positions of atoms in space but exposes information related to all electron−electron interactions present in the molecule. Furthermore, many different electron−electron interactions can contribute to the same region of the intracule or extracule space, which introduces an additional difficulty for a proper interpretation of their topological features. Therefore, although it has been shown that $\nabla^2 I(\mathbf{r})$ and $\nabla^2 E(\mathbf{R})$ distributions can be much more

* Corresponding authors.
† Tel.: +34 972 418364. Fax: +34 972 418356. E-mail: quel@iqc.udg.es.
‡ Tel.: +31 412 661456. Fax: +31 412 662539. E-mail: j.mestres@organon.oss.akzonobel.nl.

10.1021/jp001741p CCC: $19.00
Published on Web 08/19/2000

revealing than $I(\mathbf{r})$ and $E(\mathbf{R})$ distributions,[13] the difficulty of interpretation of these topological maps is still their major drawback.

The main objective of this work is to make an interpretation *à la* VB of the topology of molecular $I(\mathbf{r})$, $E(\mathbf{R})$, $\nabla^2 I(\mathbf{r})$, and $\nabla^2 E(\mathbf{R})$ distributions obtained at the HF and CISD levels of theory. In chemistry, the analysis of molecular systems in terms of valence bond (VB) structures is a very intuitive way of interpreting the electronic characteristics of molecules on the basis of electron-pair reorganizations.[16,17] Thus, it seems obvious that reasoning in terms of VB structures may represent a simple and useful means for interpreting the topology of electron-pair distributions. The following sections contain, first, a description of the computational methodology used, followed by an application to the H_2 and linear H_3^+ two-electron systems and their respective dissociation reactions, $H_2 \rightarrow H^\bullet + H^\bullet$ and $H_3^+ \rightarrow H_2 + H^+$.

Computational Details

Geometries for the H_2 and linear H_3^+ molecules were optimized at the CISD level using the 6-311G basis set. Then, HF wave functions were obtained at the CISD-optimized geometry using the same basis set. In all cases, the resulting molecular coordinates were mass-centered and the molecules aligned along the z axis. All $I(\mathbf{r})$, $E(\mathbf{R})$, $\nabla^2 I(\mathbf{r})$, and $\nabla^2 E(\mathbf{R})$ distributions from HF and CISD wave functions were computed following the algorithm described by Cioslowski and Liu,[11] using an integral neglect threshold of 10^{-8}. The center of all intracule and extracule distributions was positioned at the origin of their respective coordinates. Then, calculation of intracule and extracule topological maps on the $x-z$ plane was extended ± 3.0 and ± 1.5 au, respectively, for the H_2 molecule, and ± 4.0 and ± 2.0 au, respectively, for the linear H_3^+ molecule. For both molecules, grid steps of 0.1 and 0.05 au were used for all intracule and extracule calculations, respectively. In all maps, minima and maxima along the molecular axis were located using a grid step of 0.001 au. The contribution of each of the H^-H^+, H^+H^-, and $H^\bullet H^\bullet$ VB structures to the HF and CISD molecular wave functions was calculated following the method described in ref 18.

For the dissociation reaction of the H_2 molecule, $H_2 \rightarrow H^\bullet + H^\bullet$, HF and CISD wave functions were computed at H−H distances between 0.8 and 2.0 Å, with a grid step of 0.1 Å. The contribution of each VB structure to the HF and CISD wave functions was also calculated for each H−H distance. For the dissociation reaction of the linear H_3^+ molecule, $H_3^+ \rightarrow H_2 + H^+$, the H_2−H distance was systematically varied between 0.8 and 3.0 Å, with a grid step of 0.2 Å. Under the constraint of the H_2−H distance, the geometry of the H_2 fragment at each point of the reaction coordinate was optimized at the CISD level. HF wave functions were obtained by performing single-point HF calculations at the CISD-optimized geometries. All $I(\mathbf{r})$, $E(\mathbf{R})$, $\nabla^2 I(\mathbf{r})$, and $\nabla^2 E(\mathbf{R})$ calculations were done along the molecular axis. The leftmost hydrogen atom was always taken as the coordinate origin. Then, electron-pair calculations were extended up to 4.0 and 8.0 au for the H_2 and linear H_3^+ dissociations, respectively, using a grid step of 0.001 au. The assignment of $I(\mathbf{r})$ and $E(\mathbf{R})$ values to the different VB structures along the reaction coordinate was performed by localizing local maxima and minima on the molecular axis in the $\nabla^2 I(\mathbf{r})$ and $\nabla^2 E(\mathbf{R})$ difference maps between HF and CISD (HF-CISD). All HF and CISD calculations were performed using the Gamess[19] and Gaussian 94 packages.[20]

Results and Discussion

The H_2 and linear H_3^+ molecules have been selected as illustrative examples. The fact that these molecular systems have only two electrons makes them especially suitable to present the interpretation *à la* VB of electron-pair density and Laplacian distributions proposed in this work and discuss in detail the different interpretation of intracule and extracule distributions. Furthermore,in order to show the applicability of intracule and extracule distributions to the analysis of chemical reactivity in terms of VB structures, the dissociations of the H_2 molecule into two $H^\bullet$ atoms, $H_2 \rightarrow H^\bullet + H^\bullet$, and the linear H_3^+ molecule into H_2 and H^+, $H_3^+ \rightarrow H_2 + H^+$, will be studied.

H_2. The H_2 molecule is the simplest two-electron molecular system that can be considered. Therefore, it will be used to introduce the VB interpretation of intracule and extracule distributions. There are only three possible ways of organizing the single electron pair of the H_2 molecule on its two H atoms, which leads to three VB structures: two ionic, H^-H^+ and H^+H^-, and one covalent, $H^\bullet H^\bullet$. The aim of this section is to assess the possibility of recognizing each one of these VB structures in the topology of $I(\mathbf{r})$, $E(\mathbf{R})$, and their respective Laplacian distributions.

The set of $I(\mathbf{r})$ and $\nabla^2 I(\mathbf{r})$ distributions obtained at the HF and CISD levels of calculation for the H_2 molecule are depicted in Figure 1. Also shown are the $I(\mathbf{r})$ and $\nabla^2 I(\mathbf{r})$ difference maps between the HF and CISD levels. Correspondingly, the set of $E(\mathbf{R})$ and $\nabla^2 E(\mathbf{R})$ distributions obtained at the HF and CISD levels of calculation are collected in Figure 2, together with the $E(\mathbf{R})$ and $\nabla^2 E(\mathbf{R})$ difference maps between the HF and CISD levels. The topological analyses of all intracule and extracule maps are gathered in Tables1 and 2, respectively.

At the HF level, the $I(\mathbf{r})$ distribution for H_2 shows a single maximum at the origin with $I(0) = 0.038$ (Figure 1a). As noticed earlier by Thakkar et al.,[5] the HF $I(\mathbf{r})$ distribution is not isotropic but shows some degree of ellipticity along the molecular axis. At the CISD level, the $I(\mathbf{r})$ distribution for H_2 presents two maxima located at $r = \pm 0.920$ au on the z axis with $I(\mathbf{r}) = 0.027$, whereas the origin is a saddle point connecting the two maxima (Figure 1b). In fact, when using a larger basis set, a minimum or cage point rather than a saddle point is found at the origin of the intracule density distribution.[21] It is well-known that, besides taking into account electron correlation, explicitly correlated basis sets at least linear in the two-electron coordinate r_{12} are needed in order to satisfy the electron−electron cusp condition[4] and obtain an accurate description of the intracule density around the origin. As orbital basis sets become larger, they should improve the intracule density about the origin as is the case here for H_2; however, wave functions so constructed cannot satisfy the cusp condition[4] as $(\partial/\partial r)I(r)$ vanishes for such wave functions. However, the fact that the topology of $I(\mathbf{r})$ is basis set dependent does not affect the rationale behind the VB interpretation of $I(\mathbf{r})$ maps proposed in this work. The difference map between the HF and CISD $I(\mathbf{r})$ distributions (Figure 1c) shows in a more visual way the local differences between the $I(\mathbf{r})$ at the two levels. In agreement with a previous study by Wang et al.,[7] it is found that values of $I(\mathbf{r})$ are larger at the HF level than at the CISD level in the region surrounding the origin of the intracule coordinate. Following the molecule axis, the difference between the values of $I(\mathbf{r})$ at the HF and CISD levels decreases until a point where they become smaller at the HF level than at the CISD level, reaching a topological minimum at $r = \pm 1.956$ au (see Table 1).

With respect to the $\nabla^2 I(\mathbf{r})$ distributions, the HF $\nabla^2 I(\mathbf{r})$ distribution (Figure 1d) evidences, even more clearly than the

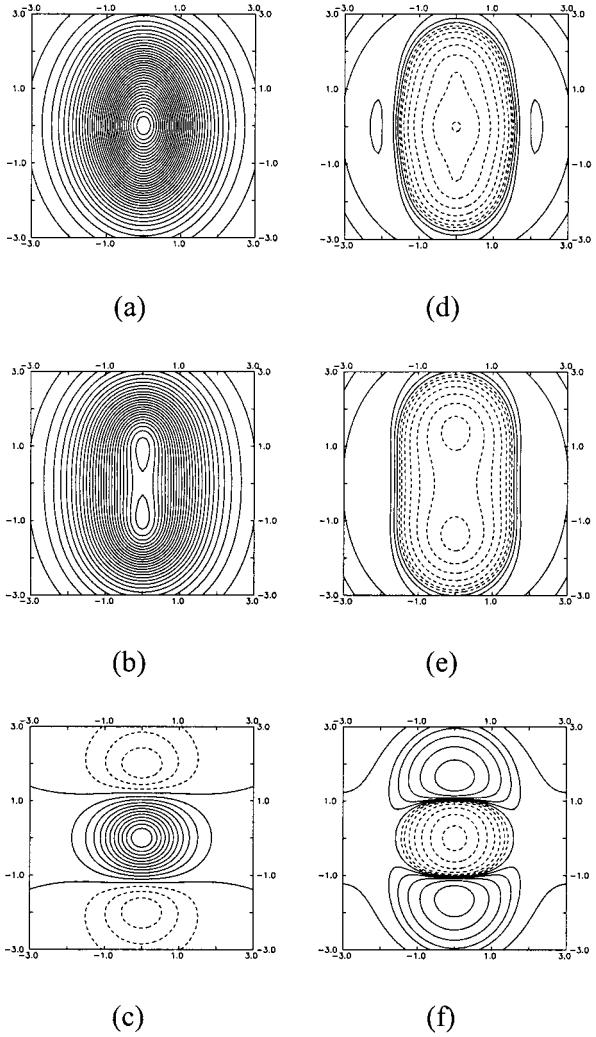

Figure 1. Intracule maps for the H_2 molecule. Positive values are depicted in solid lines and negative values in dashed lines. (a) HF $I(\mathbf{r})$ (in contours of 0.001 au). (b) CISD $I(\mathbf{r})$ (in contours of 0.001 au). (c) (HF-CISD) $I(\mathbf{r})$ (in contours of 0.001 au). (d) HF $\nabla^2 I(\mathbf{r})$ (in contours of $\pm 0.001 \times 2^n$ au, $n = 1, 2, 3, ...$). (e) CISD $\nabla^2 I(\mathbf{r})$ (in contours of $\pm 0.001 \times 2^n$ au, $n = 1, 2, 3, ...$). (f) (HF-CISD) $\nabla^2 I(\mathbf{r})$ (in contours of $\pm 0.001 \times 2^n$ au, $n = 1, 2, 3, ...$).

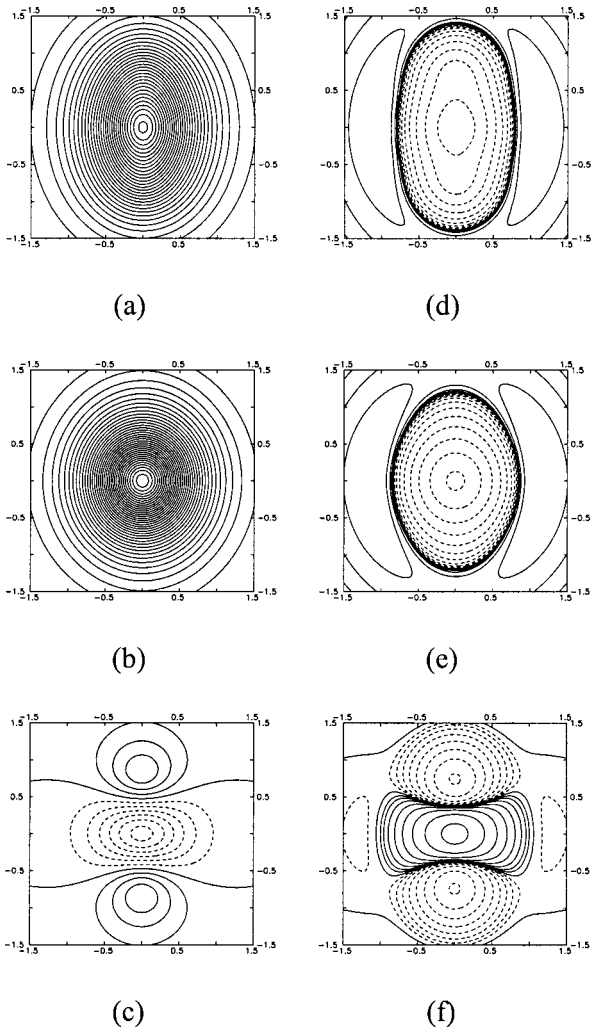

Figure 2. Extracule maps for the H_2 molecule. Positive values are depicted in solid lines and negative values in dashed lines. (a) HF $E(\mathbf{R})$ (in contours of 0.01 au). (b) CISD $E(\mathbf{R})$ (in contours of 0.01 au). (c) (HF-CISD) $E(\mathbf{R})$ (in contours of 0.01 au). (d) HF $\nabla^2 E(\mathbf{R})$ (in contours of $\pm 0.01 \times 2^n$ au, $n = 1, 2, 3, ...$). (e) CISD $\nabla^2 E(\mathbf{R})$ (in contours of $\pm 0.01 \times 2^n$ au, $n = 1, 2, 3, ...$). (f) (HF-CISD) $\nabla^2 E(\mathbf{R})$ (in contours of $\pm 0.01 \times 2^n$ au, $n = 1, 2, 3, ...$).

original HF $I(\mathbf{r})$ distribution, an anisotropic local concentration of $I(\mathbf{r})$ density from the origin along the molecule axis. Inclusion of electron correlation at the CISD level results in a $\nabla^2 I(\mathbf{r})$ distribution with two minima or points of maximum local concentration of $I(\mathbf{r})$ located at $r = \pm 1.438$ au (Figure 1e). Finally, in the line of what was found for the $I(\mathbf{r})$ distributions but contrary in sign, the difference map between $\nabla^2 I(\mathbf{r})$ distributions at the HF and CISD levels (Figure 1f) presents three topological extrema, one minimum at the origin and two maxima at $r = \pm 1.605$ au (see Table 1).

As observed for $I(\mathbf{r})$, the $E(\mathbf{R})$ distribution at the HF level shows also some degree of ellipticity along the molecular axis from its single maximum at the origin (Figure 2a). However, in contrast with what was found before for $I(\mathbf{r})$, the $E(\mathbf{R})$ map at the CISD level has practically a spherical distribution around a single maximum at the origin (Figure 2b). The difference map between the HF and CISD $E(\mathbf{R})$ distributions (Figure 2c) reveals more clearly the local differences between the $E(\mathbf{R})$ at the two levels. Also in agreement with a previous study by Wang et al.,[7] it is found that the $E(\mathbf{R})$ difference map is complementary to the $I(\mathbf{r})$ difference map, with a minimum at the origin and two maxima at $r = \pm 0.848$ au (see Table 2).

TABLE 1: Attractors in the Intracule Maps for the H_2 Molecule

	minima		maxima	
map	z (au)	value (au)	z (au)	value (au)
$I(\mathbf{r})$ HF			0.000	0.0379
$I(\mathbf{r})$ CISD			± 0.920	0.0265
$I(\mathbf{r})$ (HF-CISD)	± 1.956	-0.00368	0.000	0.0120
$\nabla^2 I(\mathbf{r})$ HF	0.000	-0.133		
$\nabla^2 I(\mathbf{r})$ CISD	± 1.438	-0.0882		
$\nabla^2 I(\mathbf{r})$ (HF-CISD)	0.000	-0.0884	± 1.605	0.0263

The HF $\nabla^2 E(\mathbf{R})$ distribution (Figure 2d) reveals an anisotropic local concentration of $E(\mathbf{R})$ density from the origin along the molecule axis, comparable to the previously shown $\nabla^2 I(\mathbf{r})$ distribution. However, in contrast with $\nabla^2 I(\mathbf{r})$, inclusion of electron correlation at the CISD level results in a $\nabla^2 E(\mathbf{R})$ distribution with a single minimum at the origin (Figure 2e). Finally, the difference map between $\nabla^2 E(\mathbf{R})$ distributions at the HF and CISD levels (Figure 2f) presents three topological extrema, one maximum at the origin and two minima at $r = \pm 0.743$ au (see Table 2).

Up to this point, the topological features of $I(\mathbf{r})$, $E(\mathbf{R})$, $\nabla^2 I(\mathbf{r})$, and $\nabla^2 E(\mathbf{R})$ distributions have been only described and com-

TABLE 2: Attractors in the Extracule Maps for the H_2 Molecule

	minima		maxima	
map	z (au)	value (au)	z (au)	value (au)
$E(\mathbf{R})$ HF			0.000	0.303
$E(\mathbf{R})$ CISD			0.000	0.367
$E(\mathbf{R})$ (HF-CISD)	0.000	−0.0643	±0.848	0.0373
$\nabla^2E(\mathbf{R})$ HF	0.000	−4.262		
$\nabla^2E(\mathbf{R})$ CISD	0.000	−5.940		
$\nabla^2E(\mathbf{R})$ (HF-CISD)	±0.743	−1.395	0.000	1.678

pared but they have not been interpreted yet. Focusing now on this last aspect, it may be worth recalling at this stage that each point in $I(\mathbf{r})$ distributions represents the probability density of finding an electron pair at a given electron−electron distance, whereas in $E(\mathbf{R})$ distributions each point represents the probability density of finding the center of mass of an electron pair at that position. With this fact in mind, one can associate the positions of extrema at internuclear distances in intracule maps and at internuclear centers of mass in extracule maps to one, or a group, of the VB structures mentioned above. This idea is schematically given below, where the VB structure(s) at the center are associated with the origin in the respective maps in Figures 1 and 2.

intracule maps	extracule maps
$H^{\bullet}H^{\bullet}$	H^-H^+
H^-H^+, H^+H^-	$H^{\bullet}H^{\bullet}$
$H^{\bullet}H^{\bullet}$	H^+H^-

Therefore, in principle, three extrema should be present in all $I(\mathbf{r})$, $E(\mathbf{R})$, $\nabla^2I(\mathbf{r})$, and $\nabla^2E(\mathbf{R})$ distributions. However, it has been already seen from Figures 1 and 2 that this is not always the case. An analysis *à la* VB of intracule and extracule distributions may help to interpret their topological features and to understand that although in some cases their topology can be very similar (compare for instance Figures 1a and 2a) their interpretation is essentially different (vide infra).

The contributions to the total wave function of each one of the VB structures representing the H_2 molecule can be obtained from VB calculations.[22] For the H^-H^+, H^+H^-, and $H^{\bullet}H^{\bullet}$ structures the contributions at the HF level are 25%, 25%, and 50%, respectively, whereas at the CISD level, they become 11%, 11%, and 78%, respectively. Within this scheme, a simple rationale for the presence or absence of each VB structure as a topological extreme in each of the maps in Figures 1 and 2 can be derived. As illustrated below, this can be done by assigning the expected percentage of contribution of each VB structure to the corresponding positions in intracule and extracule maps.

intracule	HF	CISD	HF-CISD
$H^{\bullet}H^{\bullet}$	25%	39%	−14%
H^-H^+, H^+H^-	50%	22%	+28%
$H^{\bullet}H^{\bullet}$	25%	39%	−14%
Figure	1a	1b	1c
extracule	HF	CISD	HF-CISD
H^-H^+	25%	11%	−14%
$H^{\bullet}H^{\bullet}$	50%	78%	+28%
H^+H^-	25%	11%	−14%
Figure	2a	2b	2c

As revealed by VB calculations, ionic structures are exaggerated at the HF level. On top of that, due to the definition of the intracule coordinate, in the intracule density presented in Figure 1a the two ionic structures contribute to the origin and the covalent structure actually splits its contribution into two different regions in space. This results in a single topological maximum at the origin for the H_2 intracule density that can be associated with the two ionic structures. In contrast, each VB structure contributes to a different region of the space in the extracule density in Figure 2a. In this case, the single topological maximum at the origin for the H_2 extracule density can be associated with the covalent structure. Note that the percentages of contribution of the different VB structures to the different positions in space in the extracule density are similar to those found in the intracule density (50% at the origin, and 25% on the two sides). In fact, visual comparison of the intracule and extracule density maps in Figures 1a and 2a reveals that they have approximately the same degree of ellipticity, in agreement with the qualitative reasoning given above based on the percentages of contribution of the different VB structures. Therefore, despite their evident topological similarity, it is important to remark that their interpretation in terms of VB structures is essentially different.

Calculation of the contributions of the VB structures to the wave function at the CISD level gives a larger weight to the covalent structure (78%) with respect to the two ionic structures (11% each). Promoting the contribution of the covalent structure from 50% to 78% has a substantial effect on the topology of the intracule and extracule densities. On one hand, even though the two ionic structures contribute to the origin of the intracule density in Figure 1b, the sum of their contributions (22%) is not large enough to hide the split contribution of the covalent structure on both sides (39%). With respect to the HF map, the origin of the CISD intracule density is a saddle point connecting the two maxima associated with the split contributions of the covalent structure. Moreover, the larger contribution of the covalent structure to the origin of the CISD extracule density in Figure 2b is translated in a significant reduction of the ellipticity observed in the HF map.

The same simple rationale based on the contributions of the VB stuctures to the HF and CISD wave functions can be used to qualitatively understand the differences in sign of the intracule and extracule HF-CISD difference maps in Figures 1c and 2c. Exaggeration of the contribution of ionic structures at the HF level results in positive values at the origin and negative values at the sides in the intracule density difference map in Figure 1c and negative values at the origin and positive values at the sides in the extracule density difference map in Figure 2c. In turn, an analysis of the HF-CISD difference Laplacian maps in Figures 1f and 2f reveals that the exaggeration of the ionic contributions at the HF level of theory results in negative values at the origin and negative values at the sides in the $\nabla^2I(\mathbf{r})$ difference map, while the opposite holds for the $\nabla^2E(\mathbf{R})$ difference map.

Finally, it is interesting to compare the positions of the topological extrema associated with the covalent structure in the CISD intracule density and Laplacian maps and also in the four difference maps with the actual H−H distance of 1.506 au (see Table 1). This value differs quite significantly from the positions of the two maxima found in the CISD $I(\mathbf{r})$ map in Figure 1b, located at ±0.920 au. This is due to the attractive effect that the sum of contributions of the ionic structures at the origin (22%) has on the split contributions of the covalent structure (39%) in the CISD intracule density. In contrast, the positions of the two minima found in the CISD $\nabla^2I(\mathbf{r})$ distribution in Figure 1e, located at ±1.438 au, do not correspond exactly with the positions of the two maxima found in the original CISD $I(\mathbf{r})$ density, located at ±0.920 au, and are much closer to the actual value of the H−H distance, 1.506 au.

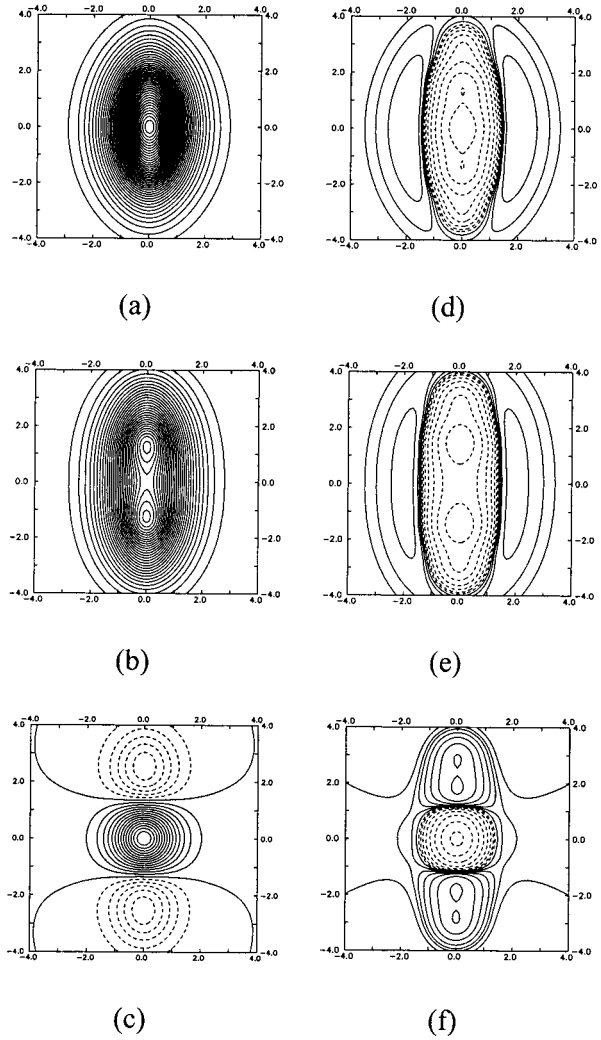

Figure 3. Intracule maps for the linear H_3^+ molecule. Positive values are depicted in solid lines and negative values in dashed lines. (a) HF $I(\mathbf{r})$ (in contours of 0.001 au). (b) CISD $I(\mathbf{r})$ (in contours of 0.001 au). (c) (HF-CISD) $I(\mathbf{r})$ (in contours of 0.001 au). (d) HF $\nabla^2 I(\mathbf{r})$ (in contours of $\pm 0.001 \times 1.914^n$ au, $n = 1, 2, 3, ...$). (e) CISD $\nabla^2 I(\mathbf{r})$ (in contours of $\pm 0.001 \times 2.000^n$ au, $n = 1, 2, 3, ...$). (f) (HF-CISD) $\nabla^2 I(\mathbf{r})$ (in contours of $\pm 0.001 \times 1.888^n$ au, $n = 1, 2, 3, ...$).

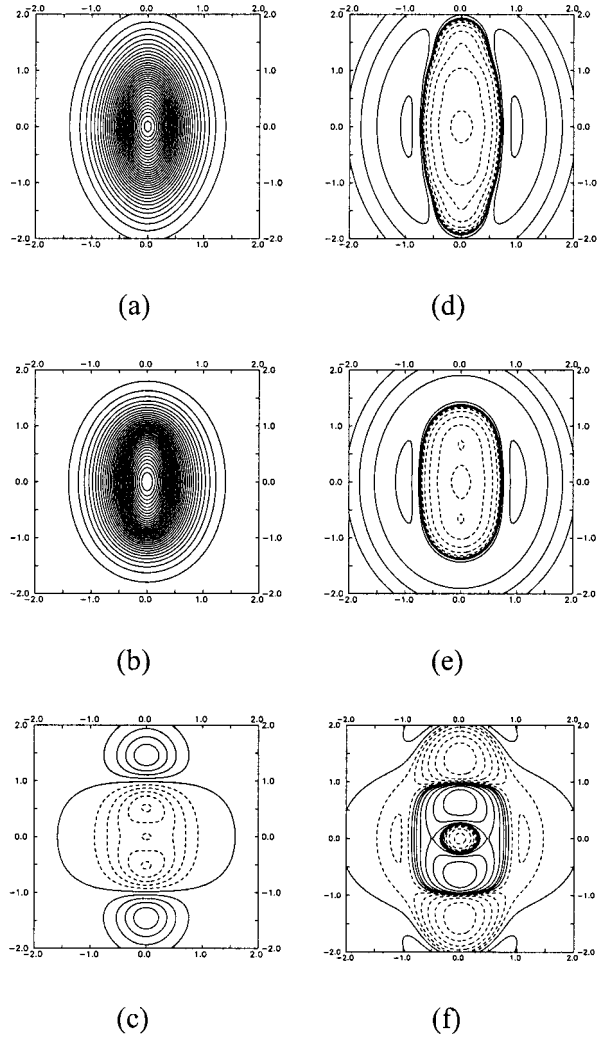

Figure 4. Extracule maps for the linear H_3^+ molecule. Positive values are depicted in solid lines and negative values in dashed lines. (a) HF $E(\mathbf{R})$ (in contours of 0.01 au). (b) CISD $E(\mathbf{R})$ (in contours of 0.01 au). (c) (HF-CISD) $E(\mathbf{R})$ (in contours of 0.005 au. (d) HF $\nabla^2 E(\mathbf{R})$ (in contours of $\pm 0.01 \times 2.655^n$ au, $n = 1, 2, 3, ...$). (e) CISD $\nabla^2 E(\mathbf{R})$ (in contours of $\pm 0.01 \times 2.661^n$ au, $n = 1, 2, 3, ...$). (f) (HF-CISD) $\nabla^2 E(\mathbf{R})$ (in contours of $\pm 0.01 \times 2.000^n$ au, $n = 1, 2, 3, ...$).

Therefore, on one side, from the CISD $I(\mathbf{r})$ map one can deduce that the maximum probability of an electron−electron interaction for the H_2 molecule is found at a distance of 0.920 au and, on the other side, from the CISD $\nabla^2 I(\mathbf{r})$ map one obtains that it is actually at a distance of 1.438 au where the strongest local concentration of that probability takes place, the latter being much closer to the actual H−H distance. This dichotomy can only be understood if one considers that each electron−electron interaction contributes to a region in intracule space, rather than to a single point. Therefore, local maxima in $I(\mathbf{r})$ may reflect the contribution of several electron−electron interactions, and be found relatively far away from the positions expected according to internuclear distances. On the other hand, $\nabla^2 I(\mathbf{r})$ distributions reflect local concentrations of intracule density. Thus, the contribution of a single VB structure is more easily reflected as a local extrema in $\nabla^2 I(\mathbf{r})$ rather than in $I(\mathbf{r})$ distributions.

Linear H_3^+. The same interpretative scheme introduced for H_2 will be applied now to the linear H_3^+ molecule. The set of $I(\mathbf{r})$ and $\nabla^2 I(\mathbf{r})$ distributions obtained for H_3^+ at the HF and CISD levels are depicted in Figure 3, including difference maps between HF and CISD density and Laplacian distributions.

TABLE 3: Attractors in the Intracule Maps for the Linear H_3^+ Molecule

	minima		maxima	
map	z (au)	value (au)	z (au)	value (au)
$I(\mathbf{r})$ HF			0.000	0.0418
$I(\mathbf{r})$ CISD			±1.255	0.0294
$I(\mathbf{r})$ (HF-CISD)	±2.544	−0.00568	0.000	0.0150
$\nabla^2 I(\mathbf{r})$ HF	0.000	−0.156		
	±1.353	−0.0956		
$\nabla^2 I(\mathbf{r})$ CISD	±1.492	−0.114		
$\nabla^2 I(\mathbf{r})$ (HF-CISD)	0.000	−0.103	±1.817	0.0262
			±2.874	0.0252

Correspondingly, the set of HF and CISD $E(\mathbf{R})$ and $\nabla^2 E(\mathbf{R})$ maps, together with the $E(\mathbf{R})$ and $\nabla^2 E(\mathbf{R})$ difference maps, are presented in Figure 4. The attractors located in all the intracule and extracule distributions are reported in Tables 3 and 4.

In the case of the linear H_3^+ molecule, there are six possible ways of distributing two electrons between three H atoms, leading to a total number of six VB structures: three ionic structures, $H^-H^+H^+$, $H^+H^-H^+$, and $H^+H^+H^-$, two short-range covalent structures, $H^\bullet H^\bullet H^+$ and $H^+H^\bullet H^\bullet$, and a long-range covalent structure, $H^\bullet H^+H^\bullet$. The expected position of these

TABLE 4: Attractors in the Extracule Maps for the Linear H_3^+ Molecule

	minima		maxima	
map	z (au)	value (au)	z (au)	value (au)
$E(\mathbf{R})$ HF			0.000	0.334
$E(\mathbf{R})$ CISD			0.000	0.349
$E(\mathbf{R})$ (HF-CISD)	±0.518	−0.0255	0.000	−0.0146
			±1.454	0.0240
$\nabla^2E(\mathbf{R})$ HF	0.000	−4.993		
	±0.677	−3.061		
$\nabla^2E(\mathbf{R})$ CISD	0.000	−4.562	±1.593	0.125
	±0.678	−3.667		
$\nabla^2E(\mathbf{R})$ (HF-CISD)	0.000	−4.314	±0.682	0.606
	±1.440	−0.615		

different VB structures in the intracule and extracule maps in Figures 3 and 4 is shown in the following scheme, where the structures at the center correspond to the origin of the maps:

intracule maps	extracule maps
$H^{\bullet}H^+H^{\bullet}$	$H^-H^+H^+$
$H^{\bullet}H^{\bullet}H^+$, $H^+H^{\bullet}H^{\bullet}$	$H^{\bullet}H^{\bullet}H^+$
$H^-H^+H^+$, $H^+H^-H^+$, $H^+H^+H^-$	$H^+H^-H^+$, $H^{\bullet}H^+H^{\bullet}$
$H^{\bullet}H^{\bullet}H^+$, $H^+H^{\bullet}H^{\bullet}$	$H^+H^{\bullet}H^{\bullet}$
$H^{\bullet}H^+H^{\bullet}$	$H^+H^+H^-$

This scheme clearly exhibits one of the main difficulties in interpreting properly intracule and extracule maps which is that, because of molecular symmetry, different interactions can contribute to the same region of the intracule or extracule space or, alternatively, a single interaction can split its contribution into different regions. For instance, in the intracule maps, the three ionic structures ($H^-H^+H^+$, $H^+H^-H^+$, and $H^+H^+H^-$) contribute collectively to a particular region in intracule space, whereas the two short-range covalent structures ($H^{\bullet}H^{\bullet}H^+$ and $H^+H^{\bullet}H^{\bullet}$) contribute collectively to two different regions in the intracule space, and the contribution of the long-range covalent structure ($H^{\bullet}H^+H^{\bullet}$) is split into the two outmost regions in intracule space. In contrast, in the extracule maps, there are four VB structures ($H^-H^+H^+$, $H^+H^+H^-$, $H^{\bullet}H^{\bullet}H^+$, and $H^+H^{\bullet}H^{\bullet}$) that can be independently located in different regions of the extracule space, while one of the ionic structures ($H^+H^-H^+$) and the long-range covalent structure ($H^{\bullet}H^+H^{\bullet}$) contribute together to the origin of the extracule space. Intracule and extracule density maps are, therefore, complementary to each other. For this molecule, there is no local maximum or minimum in the intracule or extracule maps which can be associated only to the ($H^+H^-H^+$) VB structure.

A first visual inspection to the $I(\mathbf{r})$ and $E(\mathbf{R})$ maps at the HF and CISD levels in Figures 3 and 4 reveals that the topology of some of the density and Laplacian distributions for the linear H_3^+ looks in principle quite similar to that found for H_2. However, according to the scheme proposed above, five local extrema should be identified in each intracule and extracule map of the linear H_3^+ molecule. An interpretation *à la* VB for all these maps provides a simple rationale for the observed topology (vide infra).

In the $I(\mathbf{r})$ map at the HF level (Figure 3a), the presence of a single maximum at the origin can be related to the fact that, besides the well-known exaggeration of ionic structures at the HF level, the three ionic structures contribute collectively to the origin of the map. At the HF level, the contributions of the covalent structures, split into four different regions of the intracule space, are not important enough to yield separate maxima. Upon consideration of Coulomb correlation at the CISD level, the importance of the contribution of the covalent structures relative to that of the ionic structures increases significantly and two maxima (associated with the $H^{\bullet}H^{\bullet}H^+$ and $H^+H^{\bullet}H^{\bullet}$ structures) appear now at $r = \pm 1.255$ au flanking the origin, which becomes a saddle point (Figure 3b). The $I(\mathbf{r})$ difference map between the HF and CISD levels (Figure 3c) presents positive values in the region around the origin furnished by the ionic structures and negative values in the outmost regions where the contributions of the covalent structures are expected, with minima located at $r = \pm 2.544$ au (see Table 3), in agreement with a promotion of the contribution of covalent structures with respect to that of ionic structures when Coulomb correlation is introduced.

With respect to the $I(\mathbf{r})$ map, the $\nabla^2 I(\mathbf{r})$ map at the HF level (Figure 3d) shows, besides a minimum at the origin (which corresponds to the contribution of the three ionic structures), a pair of minima located at $r = \pm 1.353$ au, which reflect the contribution of the short-range covalent structures. However, at the CISD level, the $\nabla^2 I(\mathbf{r})$ map (Figure 3e) shows only the two minima at $r = \pm 1.492$ au which are associated with the covalent interactions, whereas the minimum at the origin has evolved into a saddle point, as observed before for the corresponding $I(\mathbf{r})$ map. Finally, the $\nabla^2 I(\mathbf{r})$ difference map between the HF and CISD levels (Figure 3f) is able to reveal each one of the extrema expected a priori in the VB scheme proposed above, with a minimum at the origin, associated with the contribution of the three ionic structures, and two pairs of maxima located at $r = \pm 1.817$ au and $r = \pm 2.874$ au, associated with the contributions of the short-range and long-range covalent structures, respectively (see Table 3), in agreement again with a promotion of the contribution of covalent structures with respect to that of ionic structures when Coulomb correlation is introduced.

In the $E(\mathbf{R})$ map at the HF level (Figure 4a), the only maximum located at the origin is expected to be furnished mainly by the ionic $H^+H^-H^+$ structure, with a small contribution from the long-range covalent structure, $H^{\bullet}H^+H^{\bullet}$. On the other hand, the strong ellipticity observed in this map is a reflection of the exaggerated contribution of the $H^-H^+H^+$ and $H^+H^+H^-$ ionic structures at the HF level which, in extracule space, contribute to the outmost region of the map. At the CISD level, the $E(\mathbf{R})$ map (Figure 4b) presents a significant reduction of the ellipticity observed at the HF level. This effect can be associated with the loss of weight of the $H^-H^+H^+$ and $H^+H^+H^-$ ionic structures upon inclusion of Coulomb correlation. The $E(\mathbf{R})$ difference map between the HF and CISD levels (Figure 4c) shows positive values located at $r = \pm 1.454$ au in the outmost regions, where the $H^-H^+H^+$ and $H^+H^+H^-$ ionic structures contribute, and negative values in the region around the origin. The short-range covalent structures contribute to a point at $r = \pm 0.518$ au included in this latter region, whereas the structures $H^+H^-H^+$ and $H^{\bullet}H^+H^{\bullet}$ both contribute to the origin, also included in the negative region. With respect to the HF aproximation, it is expected that CISD will increase the contribution of $H^{\bullet}H^+H^{\bullet}$, but decrease that of $H^+H^-H^+$. These opposed contributions to the origin of the $E(\mathbf{R})$ difference map are reflected as a local maximum within the region of negative HF-CISD $E(\mathbf{R})$ values (see Table 4).

The $\nabla^2 E(\mathbf{R})$ maps at the HF (Figure 4d) and CISD (Figure 4e) levels of theory both show a minimum at the origin, furnished by the $H^+H^-H^+$ and $H^{\bullet}H^+H^{\bullet}$ structures, and a pair of local maxima located at $r = \pm 0.677$ au and $r = \pm 0.678$ au at HF and CISD, respectively, within the region of negative values, which correspond to local concentration of $E(\mathbf{R})$ associated with the contributions of the short-range covalent structures. Although not apparent visually, the topology of the

CISD $\nabla^2 E(\mathbf{R})$ map (Figure 4e) has an additional pair of maxima located at $r = \pm 1.593$ au, which are associated with the $H^-H^+H^+$ and $H^+H^+H^-$ ionic structures. However, these maxima are found in the region where $\nabla^2 E(\mathbf{R})$ has positive values, reflecting a local depletion in $E(\mathbf{R})$ values at the CISD level in this region. Finally, as observed previously in the $\nabla^2 I(\mathbf{r})$ difference map (Figure 3f), the $\nabla^2 E(\mathbf{R})$ difference map between the HF and CISD levels (Figure 4f) is able to reveal each one of the extrema expected a priori in the VB scheme proposed above. In this case, the region around the origin contains negative values, reflecting a higher local concentration of $E(\mathbf{R})$ density at the HF level than at the CISD level for this region (see Table 4). On the other hand, the $\nabla^2 E(\mathbf{R})$ difference map shows positive values in a region around $r = \pm 0.682$ au, reflecting a higher local concentration of $E(\mathbf{R})$ density at the CISD level than at the HF level for this region (see Table 4) and associated with the promotion of the contribution of the short-range covalent structures at the CISD level. The outmost region around $r = \pm 1.440$ au contains again negative values of the $\nabla^2 E(\mathbf{R})$ difference map, reflecting a higher local depletion of $E(\mathbf{R})$ density at the CISD level than at the HF level for this region (see Table 4) and associated with the promotion of the contribution of ionic structures at the HF level (see Table 4).

In the line of what was found before for the H_2 molecule, the position of the local maxima associated with the covalent interactions in the $I(\mathbf{r})$ maps are not exactly coincident with the H−H distances in the linear H_3^+ molecule. The distances between two consecutive H atoms and between the two terminal H atoms in the linear H_3^+ molecule are 1.517 and 3.033 au, respectively. The maxima present in the topology of the CISD $I(\mathbf{r})$ map (Figure 3b) and associated with the contribution of the short-range covalent interactions are located at $r = \pm 1.255$ au (see Table 3). The fact that these maxima appear at shorter distances than the short H−H distance of 1.517 au is a consequence of the overlap with the ionic structures contributing to the maximum at the origin of the $I(\mathbf{r})$ map. In contrast, in the CISD $I(\mathbf{r})$ difference map (Figure 3c) there are two symmetric minima located at $r = \pm 2.544$ au, a distance that lies within the values of the short and long H−H distances. In the HF and CISD $\nabla^2 I(\mathbf{r})$ maps (Figure 3d and 3e), the local minima associated with covalent interactions are located at $r = \pm 1.353$ au and $r = \pm 1.492$ au, respectively, much closer to the short H−H distance than the position of the extrema in the CISD $I(\mathbf{r})$ map. Finally, in the $\nabla^2 I(\mathbf{r})$ difference map (Figure 3f) there are two pairs of maxima located at $r = \pm 1.817$ au and $r = \pm 2.874$ au, respectively, which can be associated with the short and long-range covalent structures. In this case, both distances represent quite a good approximation to both the short and long H−H distances in the linear H_3^+ molecule.

$H_2 \rightarrow H^\bullet + H^\bullet$. Once the topologies of the intracule and extracule distributions for the H_2 molecule are described and interpreted in terms of VB structures, the same interpretative scheme can be applied to analyze its reaction of dissociation. The evolution of the $I(\mathbf{r})$ and $E(\mathbf{R})$ distributions during the $H_2 \rightarrow H^\bullet + H^\bullet$ dissociation has been studied previously at the HF and CISD levels of theory.[15,23−24] The VB interpretative scheme of intracule and extracule densities proposed here aims at providing a simpler, more intuitive, means for rationalizing the changes in electron-pair density along the reaction coordinate of the dissociation process.

Figure 5 shows the $-\nabla^2 I(\mathbf{r})$ distributions calculated at the HF (Figure 5a) and CISD (Figure 5b) levels, respectively, along the molecular axis (r) for values of the H−H distance (D) from 0.8 to 2.0 Å. For $D = 0.8$ Å, the H−H system is very close to

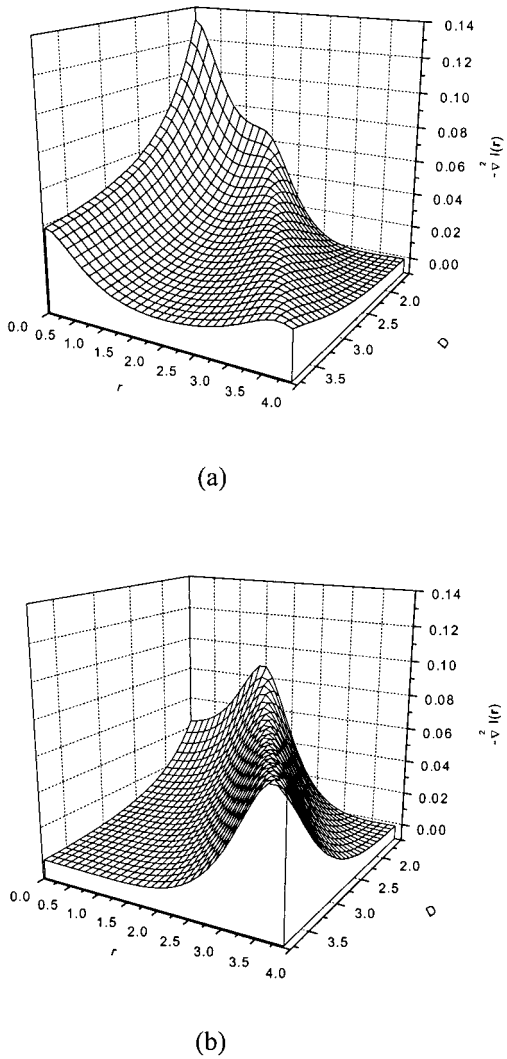

Figure 5. $\nabla^2 I(\mathbf{r})$ distributions along the molecular axis for the H_2 molecule at several H−H distances at the HF (a) and CISD (b) levels of theory. D (in au) is the H−H distance, r (in au) is the intracule coordinate on the molecular axis.

the equilibrium distance of the H_2 molecule, whereas for $D = 2.0$ Å the dissociation of H_2 into two $H^\bullet$ atoms is fairly advanced. Following the same reasoning used above for the H_2 molecule at the equilibrium distance, one can expect that, for every value of D, the ionic structures, H^-H^+ and H^+H^-, will contribute to the origin of the intracule maps, while the covalent structure, $H^\bullet H^\bullet$, will contribute to a point r corresponding approximately to the distance D. A visual comparison between the HF and CISD $-\nabla^2 I(\mathbf{r})$ distributions clearly shows that HF overestimates the contribution of ionic structures with respect to that of the covalent structure. This overestimation is carried on along the reaction coordinate as revealed by the higher local concentration of $I(\mathbf{r})$ in the origin than in the point where $r = D$, thus evidencing that this process is not described properly at the HF level (Figure 5a). In contrast, at the CISD level of theory, the value of $\nabla^2 I(\mathbf{r})$ at $r = 0$ tends to zero for large values of D, in agreement with the vanishing of the contribution of the ionic structures as the dissociation process advances. In this case, the position where $r = D$ associated with the contribution of the covalent structure is the only region where local concentration of $I(\mathbf{r})$ is still evident at large interatomic distances (Figure 5b).

The evolution of the CISD $I(\mathbf{r})$ and $E(\mathbf{R})$ values at those points associated with the contributions of the ionic and covalent structures along the reaction coordinate can be followed in

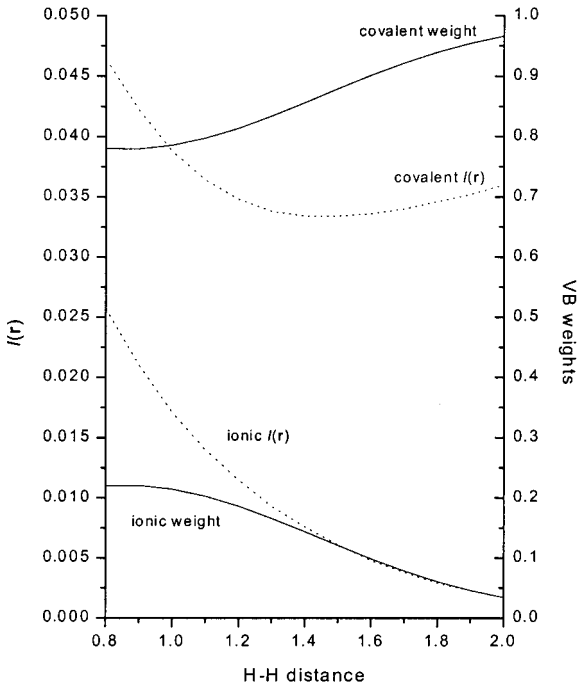

(a)

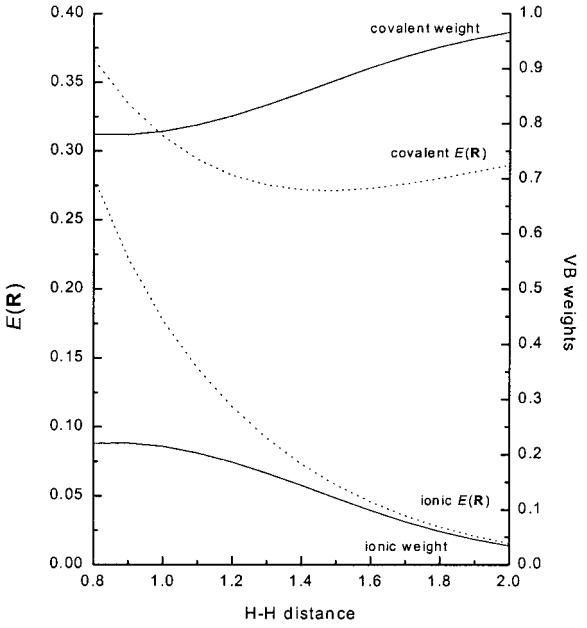

(b)

Figure 6. $I(\mathbf{r})$ (a) and $E(\mathbf{R})$ (b) values (in au, dotted lines) associated with the ionic and covalent VB structures of the H_2 molecule for different H−H distances (in Å), calculated at the CISD level. The ionic and covalent weights calculated for the CISD wave function at each distance are depicted as well (solid lines). For the sake of comparison to the $I(\mathbf{r})$ and $E(\mathbf{R})$ graphs, the covalent $I(\mathbf{r})$ values in Figure 6a and the ionic $E(\mathbf{R})$ values in Figure 6b are scaled by 2.

Figure 6. For comparison, the corresponding weights to the wave function for the ionic and covalent structures are also included. Since the covalent structure contributes to two regions in the $I(\mathbf{r})$ density map (vide supra), for the sake of consistency with the weight values, the $I(\mathbf{r})$ value at the point associated with the covalent structure was multiplied by 2 (Figure 6a). Correspondingly, since the two ionic structures contribute to two different regions in the $E(\mathbf{R})$ density map (vide supra), the $E(\mathbf{R})$ value at the point associated with one of the ionic structures was also multiplied by 2 (Figure 6b).

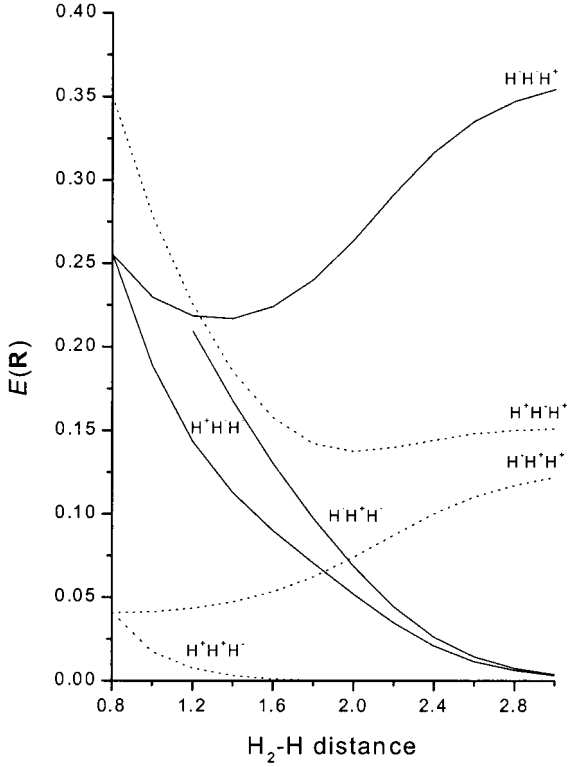

Figure 7. $E(\mathbf{R})$ values (in au) at the CISD level associated with each VB structure for the linear H_3^+ molecule at different H_2-H^+ distances (in Å). Solid and dotted lines are used for the covalent and ionic $E(\mathbf{R})$ values, respectively.

A first visual inspection to Figure 6 reveals that both the evolution of $I(\mathbf{r})$ and $E(\mathbf{R})$ values associated with the ionic and covalent structures along the reaction coordinate follow essentially the same trend. At short H−H distances (<1.5 Å), a sharp decrease in the $I(\mathbf{r})$ and $E(\mathbf{R})$ values is observed. Within this range of H−H distances, the evolution of $I(\mathbf{r})$ and $E(\mathbf{R})$ values is not in agreement with that followed by the weights. In contrast, at larger H−H distances (>1.5 Å), the evolution of $I(\mathbf{r})$ and $E(\mathbf{R})$ values follows closely that observed for the weights, especially for those values associated with the ionic structures. A rationale for this behavior can be derived when considering the strong interaction between the contributions of the different VB structures in the intracule and extracule spaces (see Figures 1b and 2b). Therefore, at short H−H distances, the evolution of the $I(\mathbf{r})$ and $E(\mathbf{R})$ values associated with the covalent and ionic structures will reflect mainly the decrease in overlap in the intracule and extracule spaces between their respective contributions rather than the genuine changes in the VB weights. At large H−H distances, as the overlap in the intracule and extracule spaces between the contributions of the covalent and ionic structures finally vanishes, the evolution of the $I(\mathbf{r})$ and $E(\mathbf{R})$ values will follow essentially the same trend observed for the actual VB weights.

$\mathbf{H_3^+ \rightarrow H_2 + H^+}$. Finally, the dissociation of the linear H_3^+ molecule into H_2 and H^+ was also studied following the evolution of the $I(\mathbf{r})$ and $E(\mathbf{R})$ values at the points in their respective distributions associated with each VB structure along the reaction coordinate. The results are presented in Figure 7. In this case, only the results obtained from the changes in the CISD $E(\mathbf{R})$ distribution along the reaction coordinate are shown

because of the better separability of the contributions of the different VB structures to the extracule space as compared to those to the intracule space (vide supra).

A first examination of the evolution of the $E(\mathbf{R})$ curves associated with each VB structure in Figure 7 reveals that the separate contribution of two of the VB structures ($H^+H^-H^+$ and $H^\bullet H^+H^\bullet$) was not possible to assign at H_2-H distances shorter than 1.3 Å. As discussed above, these two VB structures contribute collectively to the origin in extracule maps in the linear H_3^+ molecule. Accordingly, discrimination between them is not possible until the dissociation process is advanced (H_2-H distances larger than 1.3 Å). Therefore, $E(\mathbf{R})$ values assigned to the ensemble of these two structures were initially assigned arbitrarily to $H^+H^-H^+$. However, their mutual interaction continues further along the reaction coordinate until the H_2-H distance is about 2.0 Å, as can be extracted from the sharp decrease of their $E(\mathbf{R})$ curves, especially for the one associated with $H^\bullet H^+H^\bullet$. At this point of the reaction coordinate, the $E(\mathbf{R})$ curve associated with $H^+H^-H^+$ reaches a minimum, from which it will smoothly converge to the $E(\mathbf{R})$ value found in the H_2 molecule for this structure as the interaction between H_2 and H^+ diminishes, whereas the $E(\mathbf{R})$ curve associated with $H^\bullet H^+H^\bullet$ continues its sharp decrease until it practically vanishes. Although not as critical as for the $H^+H^-H^+$ and $H^\bullet H^+H^\bullet$ structures, a similar behavior is observed for the $E(\mathbf{R})$ curves associated with the two short-range covalent structures ($H^\bullet H^\bullet H^+$ and $H^+H^\bullet H^\bullet$). Due to the overlap with the VB structures contributing to the origin in extracule space, both $E(\mathbf{R})$ curves initiate a descend in value. This descend is strongly accentuated for the $E(\mathbf{R})$ curve corresponding to $H^+H^\bullet H^\bullet$, which will eventually vanish at large H_2-H distances. The $E(\mathbf{R})$ curve associated with $H^\bullet H^\bullet H^+$ reaches a minimum when the H_2-H distance is about 1.5 Å and then experiences a new increase in value until it smoothly converges to the $E(\mathbf{R})$ value found in the H_2 molecule for this structure. Finally, the two ionic structures contributing to the outmost region in extracule space ($H^+H^+H^-$ and $H^-H^+H^+$) do not seem to be as affected by the overlap with the other VB structures in extracule space at short H_2-H distances as the rest of VB structures. Consequently, while the $E(\mathbf{R})$ curve associated with the $H^+H^+H^-$ structure vanishes already at the beginning of the dissociation process, that associated with the $H^-H^+H^+$ structure increases continuously to merge, eventually, with the $E(\mathbf{R})$ curve associated with the $H^+H^-H^+$ structure. As the dissociation process comes to an end at large H_2-H distances, all $E(\mathbf{R})$ curves tend to converge to the values found for the H_2 molecule. Thus, the $E(\mathbf{R})$ curves associated with the $H^+H^+H^-$, $H^+H^\bullet H^\bullet$, and $H^\bullet H^+H^\bullet$ structures tend to vanish, whereas the $E(\mathbf{R})$ curves corresponding to the $H^-H^+H^+$, $H^+H^-H^+$, and $H^\bullet H^\bullet H^+$ structures smoothly reach the values obtained for the H^-H^+, H^+H^-, and $H^\bullet H^\bullet$ structures, respectively, in the H_2 molecule.

Conclusions

An interpretation *à la* VB for $I(\mathbf{r})$ and $E(\mathbf{R})$ distributions has been introduced. As case examples, the $I(\mathbf{r})$ and $E(\mathbf{R})$ density and Laplacian distributions for the H_2 and linear H_3^+ molecules have been analyzed in detail. It has been shown that each of the VB structures possible for these molecules can be mapped onto a region in the intracule or extracule space. Thus, the topological features present in the $I(\mathbf{r})$, $E(\mathbf{R})$, $\nabla^2 I(\mathbf{r})$, and $\nabla^2 E(\mathbf{R})$ maps of a molecule can be interpreted in terms of the different VB structures contributing to the wave function. Within this context, the relative importance of different VB structures at the HF and CISD levels of theory is reflected in the corresponding $I(\mathbf{r})$ or $E(\mathbf{R})$ density and Laplacian difference maps and the general overestimation of ionic structures at the HF level is retrieved. In addition, the same interpretative scheme has been applied to study the $H_2 \rightarrow H^\bullet + H^\bullet$ and $H_3^+ \rightarrow H_2 + H^+$ dissociation processes as described by the evolution of their respective $I(\mathbf{r})$ and $E(\mathbf{R})$ distributions along the reaction coordinate. A good qualitative agreement between the $I(\mathbf{r})$ and $E(\mathbf{R})$ curves associated with the different VB structures and their corresponding weights to the total wave function was found at advanced stages of the dissociation processes. Therefore, despite the inherent limitations found due to, on one hand, the collective contribution of several VB structures to the same region of the intracule or extracule space and, on the other hand, the overlap between the contribution of the VB structures at different regions of the intracule and extracule space, the interpretation *à la* VB of $I(\mathbf{r})$ and $E(\mathbf{R})$ distributions of molecules and chemical processes provides a simpler and more intuitive means to understand their complicated topological features. However, the extension of this kind of analysis to larger molecules will not be straightforward, due to the difficulty of identifying separately each formal electron−electron interaction in the intracule and extracule maps for systems with many electrons. More research will be needed for extracting meaningful information from molecular intracule and extracule density distributions. In particular, several approaches have been proposed recently that allow for the analysis of molecular intracule and extracule densities in terms of the effects of electron exchange and correlation on this contracted electron-pair densities.[25,26]

Acknowledgment. We are indebted to Dr. M. Solà for his assistance in the calculation of the weights of VB structures to molecular wave functions.This work was supported by the Spanish DGICYT Project No. PB98-0457-C02-01. X.F. benefits from a doctoral fellowship from the University of Girona.

References and Notes

(1) Bader, R. F. W. *Atoms in Molecules: A Quantum Theory*; Clarendon: Oxford, UK, 1990.
(2) Davidson, E. R. *Reduced Density Matrices in Quantum Chemistry*; Academic: New York, 1976.
(3) Coleman, A. J. *Int. J. Quantum Chem.* **1967**, *18*, 457.
(4) Thakkar, A. J.; Smith, V. H. *Chem. Phys. Lett.* **1976**, *42*, 476.
(5) Thakkar, A. J.; Tripathi, A. N.; Smith, V. H., Jr. *Int. J. Quantum Chem.* **1984**, *26*, 157.
(6) Sarasola, C.; Domínguez, L.; Aguado, M.; Ugalde, J. M. *J. Chem. Phys.* **1992**, *96*, 6778.
(7) Wang, J.; Tripathi, A. N.; Smith, V. H. *J. Chem. Phys.* **1992**, *97*, 9188.
(8) Wang, J.; Tripathi, A. N.; Smith, V. H. *J. Phys. B* **1993**, *26*, 205.
(9) Wang, J.; Smith, V. H.; *Int. J. Quantum Chem.* **1994**, *49*, 147.
(10) Wang, J.; Smith, V. H. *Theor. Chim. Acta* **1994**, *88*, 35.
(11) Cioslowski, J.; Liu, G. *J. Chem. Phys.* **1996**, *105*, 4151.
(12) Cioslowski, J.; Liu, G. *J. Chem. Phys.* **1996**, *105*, 8187.
(13) Fradera, X.; Duran, M.; Mestres, J. *J. Chem. Phys.* **1997**, *107*, 3576.
(14) Fradera, X.; Duran, M.; Mestres, J. *Can. J. Chem.* **2000**, *78*, 378.
(15) Fradera, X.; Duran, M.; Mestres, J. *Theor. Chem. Acc.* **1998**, *99*, 44.
(16) Shaik, S. S.; Hiberty, P. C. *Adv. Quantum Chem.* **1995**, *26*, 99.
(17) Raimondi, M.; Cooper, D. L. *Top. Curr. Chem.* **1999**, *203*, 105.
(18) Hiberty, P. C.; Leforestier, C. *J. Am. Chem. Soc.* **1978**, *100*, 2012.
(19) Schmidt, M. W.; Baldridge, K. K.; Boatz, J. A.; Elbert, S. T.; Gordon, M. S.; Jensen, J. H.; Koseki, S.; Matsunaga, N.; Nguyen, K. A.; Su, S. J.; Windus, T. L.; Dupuis, M.; Montgomery, J. A. *J. Comput. Chem.* **1993**, *14*, 1347.
(20) Frisch, M. J.; Trucks, G. W.; Schlegel, H. B.; Gill, P. M. W.; Johnson, B. G.; Robb, M. A.; Cheeseman, J. R.; Keith, T.; Petersson, G. A.; Montgomery, J. A.; Raghavachari, K.; Al-Laham, M. A.; Zakrzewski, V. G.; Ortiz, J. V.; Foresman, J. B.; Peng, C. Y.; Ayala, P. Y.; Chen, W.; Wong, M. W.; Andrés, J. L.; Replogle, E. S.; Gomperts, R.; Martin, R. L.; Fox, D. J.; Binkley, J. S.; Defrees, D. J.; Baker, J.; Stewart, J. P.; Head-Gordon, M.; Gonzalez, C.; Pople, J. A. *Gaussian 94*; Gaussian, Inc.: Pittsburgh, PA, 1995.

(21) While this paper was being prepared, the topology of $I(\mathbf{r})$ for the H_2 molecule computed at the MP2/aug-cc-pV6Z level was reported (Cioslowski, J.; Liu, G. *J. Chem. Phys.* **1999**, *110*, 1882). At this level of theory, $I(\mathbf{r})$ exhibits a correlation cage at the origin, in contrast to the CISD/6-311G results presented in this paper (Figure 1b). This turned out to be a basis-set effect rather than a level-of-theory effect as recalculation at the CISD/aug-cc-pV6Z level revealed the correlation cage of the $I(\mathbf{r})$ topology. The cage point at the origin has $I(0) = 0.0221$ and the two attractors are located at $r = \pm 1.010$ with $I(\mathbf{r}) = 0.0266$ in close agreement with the value of $I(0) = 0.0182$ and attractors located at $r = \pm 0.973$ with $I(\mathbf{r}) = 0.0282$ found at the MP2/aug-cc-pV6Z level.

(22) Because of the limitations of the program used to project the wave functions into combinations of VB structures, the VB weights reported correspond to HF and CISD calculations carried out using the STO-3G basis set instead of the 6-311G basis set used for all intracule and extacule density and Laplacian calculations. Despite the fact that the values of the VB weights will certainly depend on the basis set used, this basis-set dependency is expected not to be critical for the following discussion.

(23) Boyd, R. J.; Sarasola, C.; Ugalde, J. M. *J. Phys. B: At. Mol. Opt. Phys.* **1998**, *21*, 2555.

(24) Cioslowski, J.; Liu, G. *J. Chem. Phys.* **1999**, *111*, 3401.

(25) Lee, A. M.; Gill, P. M. W. *Chem. Phys. Lett.* **1999**, *313*, 271.

(26) Fradera, X.; Duran, M.; Mestres, J. *J. Chem. Phys.* **2000**, *113*, 2530.